A finite element formulation of muscle contraction : implementation in DIANA

A FINITE ELEMENT FORMULATION OF MUSCLE CONTRACTION

Implementation in DIANA

A.W.J. GIELEN, P.H.M. BOVENDEERD and J.D. JANSSEN
Department of Mechanical Engineering, Eindhoven University of Technology, Eindhoven, The Netherlands

Abstract. The ability to contract is a unique feature of muscular material, as compared to technical materials. The contractile stress generated by muscle cells, acts along the muscle fibre direction, and has been shown to depend on time, elapsed since activation of the cell, on fibre strain and on fibre strain rate. In this paper we combine the equation of conservation of momentum with an existing description of the constitutive behaviour of myocardial tissue and convert the resulting equations into a numerical formulation, which is implemented in DIANA. Results of simulations of several contraction experiments are shown.

Key words: biomechanics, muscle contraction

1. Introduction

The analysis of the mechanical behaviour of biological structures is complex due to the combination of complicated macroscopic geometry, fibre structure and material properties on the one hand, and the geometrically nonlinear deformations on the other. Determination of macroscopic geometry and fibre structure should be done *in vivo* preferably, using noninvasive imaging techniques such as Magnetic Resonance Imaging. Realistic description of the constitutive behaviour of biological tissue necessitates the use of mixture models, which take into account the composition of the tissue in terms of a solid, a fluid and an ion component [8]. In general, the solid component consists of networks of collagen and elastin fibres, displaying anisotropic, nonlinear, viscoelastic behaviour. In muscular tissue, the contractile properties of the force generating elements, the sarcomeres, must be added. The sarcomeres are located in elongated muscle cells, which are grouped in macroscopic fibres. The contractile stress, as generated in muscle cells, acts along the muscle fibre direction, and has been shown to depend on time, elapsed since activation of the cell, on fibre strain (i.e. sarcomere length) and on fibre strain rate (i.e. velocity of sarcomere shortening).

In this paper we start from a mathematical description of the constitutive behaviour of cardiac tissue, paying special attention to the contractile properties. Next we incorporate this description into a finite element formulation, based on the equation of conservation of momentum, and we discuss implementation in the finite element code DIANA. Finally, we show results of simulations of several contraction

G.M.A. Kusters and M.A.N. Hendriks (eds.), DIANA Computational Mechanics '94, 139-148.

experiments.

2. Constitutive behaviour of cardiac tissue

Since we focus on contractile behaviour, we neglect the fluid and ion component in the tissue, and we model cardiac tissue as a solid material, consisting of connective tissue and muscle fibres. Both components contribute to the total Cauchy stress $\boldsymbol{\sigma}$ in the tissue:

$$\boldsymbol{\sigma} = \boldsymbol{\sigma}_p + \sigma_a \mathbf{e}_1 \mathbf{e}_1 \tag{1}$$

The passive stress $\boldsymbol{\sigma}_p$ is related to deformation of the connective tissue and the muscle fibres. The uniaxial active stress $\sigma_a \mathbf{e}_1 \mathbf{e}_1$, which acts along the muscle fibre direction $\mathbf{e}_1$, is related to contraction of the muscle cells. Although the description of the constitutive behaviour has been presented before [2], we will recapitulate it below.

2.1. The contractile fibres

Experimentally, the contractile force, that is generated in the muscle cells by the sarcomeres, has been found to depend on time, the sarcomere length l_s and the velocity of shortening of the sarcomeres [4, 6, 11]. Our model for description of the contractile behaviour is an adapted version of the model presented by Arts *et al.* [1], which was based on Hill's one-dimensional three-element model [5, 6]. The latter model consists of a passive elastic element in parallel to an active element (figure 1a). We extended the passive elastic element, which originally only described the stress-strain behaviour along the fibre direction, towards a complete three-dimensional description, as shown in the next subsection. The one-dimensional active element consists of a contractile element in series with an elastic element. The length of the active element equals the sarcomere length l_s. The length of the contractile element equals l_c. The first Piola-Kirchhoff stress T_a, as generated in an active element, is transmitted by the elastic element and given by:

$$T_a = \frac{l_{s,0}}{l_s}\,\sigma_a = E_a\,T_{max}\,(l_s - l_c) \tag{2}$$

where $l_{s,0}$ represents the sarcomere length in the reference situation. The 'stiffness' of the series elastic element is equal to $E_a T_{max}$, where E_a is a constant. T_{max} depends on l_c, l_s and the time t_s that has elapsed since the moment of onset of activation:

$$T_{max} = T_1 A_l(l_c)\,A_t(t_s, l_s) \tag{3}$$

The constant T_1 is associated with the level of maximum isometric stress. The factor $A_l(l_c)$ represents the length-dependence of active stress (figure 1b):

$$A_l(l_c) = 1 + a_x(l_c - l_x) - \sqrt{(a_x(l_c - l_x))^2 + 0.01} \tag{4}$$

The constant a_x is associated with the increase of active stress as a function of sarcomere length for small ($l_c < l_x$) sarcomere lengths. At $l_c > l_x$ the active stress

TABLE I
Values of the parameters describing the constitutive behaviour of myocardial tissue.

contractile fibres						connective tissue		
T_1	110.0	kPa	t_r	75.0	ms	a_0	0.5	kPa
T_0	55.0	kPa	t_d	75.0	ms	a_1	3.0	–
E_a	20.0	μm^{-1}	v_0	0.0075	$\mu m \cdot ms^{-1}$	a_2	6.0	–
a_x	1.3	μm^{-1}	b	150.0	$ms \cdot \mu m^{-1}$	a_3	3.0	–
l_x	2.0	μm	a_T	2.0	–	a_4	5.0	kPa
l_d	−0.4	μm						

T_a levels off. The factor $A_t(t_s, l_s)$ represents the time dependence of active stress (figure 1c):

$$\begin{aligned} A_t(t_s, l_s) &= A_r(t_s)\, A_d(t_s, l_s) \\ A_r(t_s) &= 1 - \frac{1}{1 + (t_s/t_r)^4} \\ A_d(t_s, l_s) &= \begin{cases} 1 - \dfrac{1}{1 + ((t_e - t_s)/t_d)^4} & t_s \le t_e \\ 0 & t_s > t_e \end{cases} \end{aligned} \tag{5}$$

The factors $A_r(t_s)$ and $A_d(t_s, l_s)$ represent the rise and decay of active stress, with characteristic time intervals t_r and t_d, respectively. t_e denotes the total duration of the contraction which depends on l_s according to :

$$t_e = b(l_s - l_d) \tag{6}$$

The constant b governs the increase of the duration of the activation with increasing sarcomere length, and l_d denotes the extrapolated sarcomere length at which this duration equals zero. The time derivative of l_c is modeled as (figure 1d):

$$\begin{aligned} \frac{\mathrm{d}l_c}{\mathrm{d}t} &= \left(\frac{T_a - T_{max}}{T_a + T_0}\right) v_0 && T_a \le T_{max} \\ \frac{\mathrm{d}l_c}{\mathrm{d}t} &= \left(\frac{T_a - T_{max}}{T_a + T_0}\right) v_0 \exp\left(a_T \left(\frac{T_a}{T_{max}} - 1\right)\right) && T_a > T_{max} \end{aligned} \tag{7}$$

The first equation describes a hyperbolic relationship between $\mathrm{d}l_c/\mathrm{d}t$ and T_a with asymptote velocity v_0 and asymptote stress T_0. The second equation models the experimentally observed sigmoid shape of the force-velocity curve in the high-force region [5, 11]. The values of the material parameters, which were based on data derived from literature [1, 9, 11], are listed in table I.

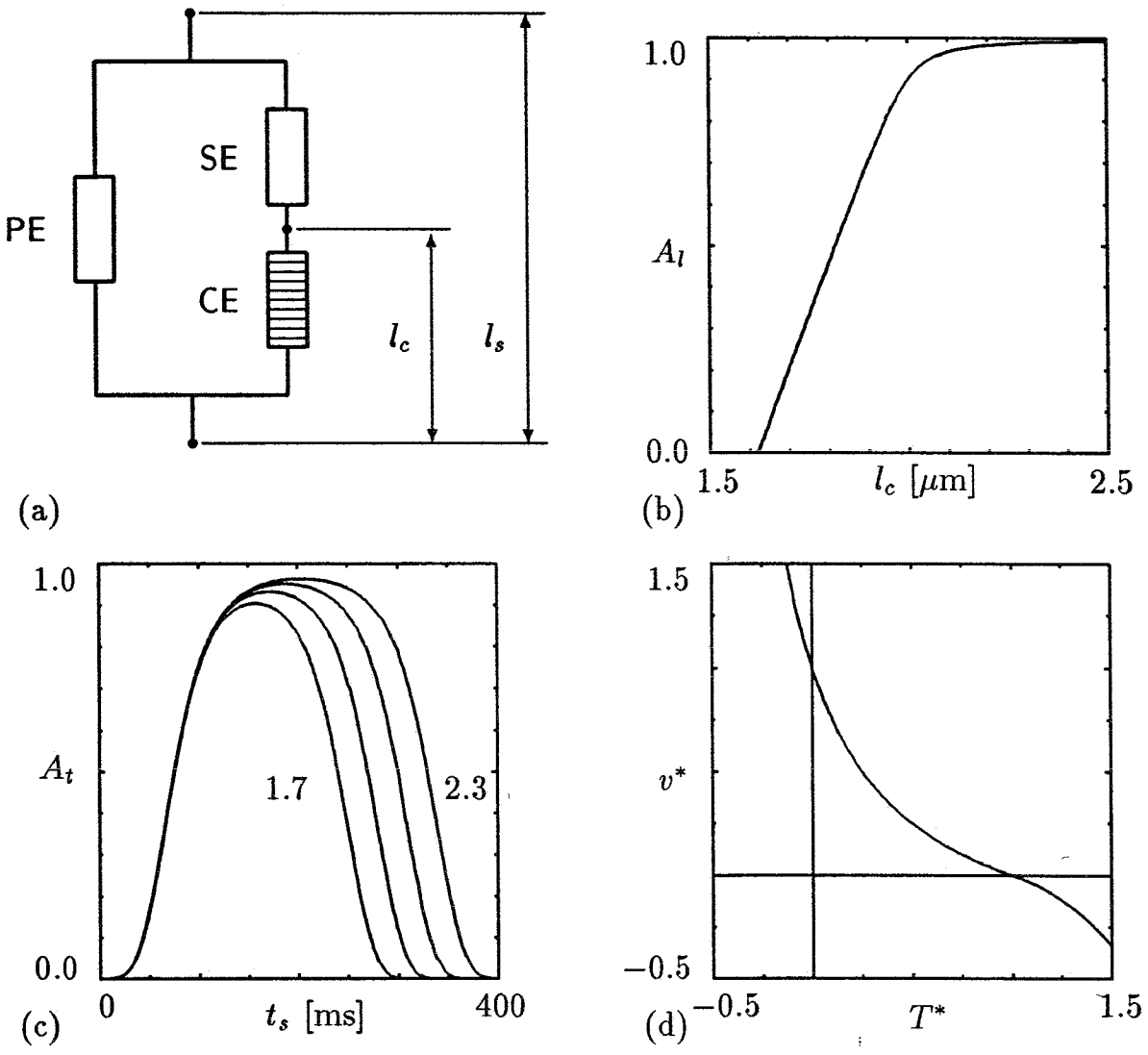

Fig. 1. Contractile material behavior: (a) three-element model with parallel elastic element PE, series elastic element SE, contractile element CE, sarcomere length l_s and contractile element length l_c; (b) length dependence of active stress, as given by equation (4); (c) time dependence of active stress, as given by equation (5), at $l_s = 1.7$, 1.9 2.1 and 2.3 μm; (d) stress-velocity relation: $v^* = -(1/v_0)(\mathrm{d}l_c/\mathrm{d}t)(T_{max}/T_0)$, $T^* = T_a/T_{max}$, as given by equation (7).

2.2. The connective tissue

The passive constitutive behaviour is described by a strain energy function $W(\boldsymbol{E})$ that relates the second Piola-Kirchhoff stress tensor $\boldsymbol{S}$ to the Green-Lagrange strain tensor $\boldsymbol{E}$:

$$\boldsymbol{S} = \partial W(\boldsymbol{E})/\partial \boldsymbol{E} \tag{8}$$

The stress tensor $\boldsymbol{S}$ is defined as:

$$\boldsymbol{S} = \det(\boldsymbol{F})\, \boldsymbol{F}^{-1} \cdot \boldsymbol{\sigma}_p \cdot \boldsymbol{F}^{-c} \tag{9}$$

where the deformation gradient tensor $\boldsymbol{F}$ describes how an infinitesimal material vector in the reference situation $d\boldsymbol{x}_0$ is transformed into a vector $d\boldsymbol{x}$ in the deformed situation:

$$d\boldsymbol{x} = \boldsymbol{F} \cdot d\boldsymbol{x}_0 \tag{10}$$

The Green-Lagrange strain tensor $\boldsymbol{E}$ is defined as:

$$\boldsymbol{E} = \tfrac{1}{2}(\boldsymbol{F}^c \cdot \boldsymbol{F} - \boldsymbol{I}) \tag{11}$$

where $\boldsymbol{I}$ represents the unity tensor. With respect to an orthonormal coordinate system with direction $\boldsymbol{e}_1$ parallel to the fibre direction and cross-fibre directions $\boldsymbol{e}_2$ and $\boldsymbol{e}_3$, the strain tensor $\boldsymbol{E}$ is written as the strain matrix $\underline{E}$ with components E_{ij}. The myocardial tissue is assumed to be transversely isotropic with respect to the fibre direction. The functional form of $W(\underline{E})$ is chosen so that (1) W and $\underline{S} = \partial W/\partial \underline{E}$ are zero in the unstrained state, (2) stress is an exponential function of strain and (3) the tissue behaves virtually incompressible. From the many strain energy functions consistent with these conditions, the following was selected:

$$W(\underline{E}) = a_0 \left[\exp(a_1\, I_E^2 + a_2\, II_E + a_3\, E_{11}^2) - 1\right] + a_4 \left[(\det(2\underline{E} - \underline{I}))^2 - 1\right]^2, \tag{12}$$

where I_E and II_E represent the first and second invariant of the Green-Lagrange strain tensor:

$$I_E = E_{11} + E_{22} + E_{33}, \tag{13}$$

$$II_E = E_{12}^2 + E_{23}^2 + E_{31}^2 - E_{11}E_{22} - E_{22}E_{33} - E_{33}E_{11}. \tag{14}$$

The first term in (12) represents stresses associated with change of shape of the tissue, while the second term enforces incompressibility to an extent which depends on the magnitude of the bulk modulus a_4. The values of the material parameters $a_0, \ldots, a_3$ were estimated using experimentally obtained data [7, 12], while the value of a_4 was chosen so as to obtain a virtually incompressible behaviour ($|\det(\boldsymbol{F}) - 1| < 10^{-3}$) in the present computations (see table I).

3. Numerical formulation

To determine the state of stress and strain in the myocardial tissue, as a result of externally applied forces and internally generated active forces, the equation of conservation of momentum has to be solved. Since the analysis is both geometrically and physically nonlinear, we choose to use the principle of weighted residuals [13] to convert this equation into a numerical formulation.

3.1. Weighted residuals formulation

Basis of the numerical formulation is the equation of conservation of momentum. Assuming no body forces and neglecting inertial and gravity effects, this equation reduces to:

$$\nabla \cdot \boldsymbol{\sigma} = \mathbf{o} \tag{15}$$

This is equivalent to:

$$\int_V \boldsymbol{h} \cdot (\nabla \cdot \boldsymbol{\sigma}) dV = 0 \tag{16}$$

where $\boldsymbol{h}$ is an arbitrary vector function and V represents the actual volume of the tissue. Using Gauss' theorem (16) transforms into:

$$\int_V \boldsymbol{\sigma} : (\nabla \boldsymbol{h})^c dV = \int_A \boldsymbol{h} \cdot \boldsymbol{\sigma} \cdot \boldsymbol{n} dA = -\int_A \boldsymbol{h} \cdot \boldsymbol{\sigma}_{ext} \cdot \boldsymbol{n} dA \tag{17}$$

The right-hand-side of (17) is associated with the externally applied traction, on the surface A of the tissue. The vector $\boldsymbol{n}$ is the normal of surface A. Transforming the equation to the undeformed (reference) configuration by using the second Piola-Kirchoff stress and defining $J = \det(\boldsymbol{F})$, yields:

$$\int_{V_0} (\nabla_0 \boldsymbol{h})^c : (\boldsymbol{S} \cdot \boldsymbol{F}^c) dV_0 = -\int_{A_0} \boldsymbol{h} \cdot \boldsymbol{\sigma}_{ext} \cdot \boldsymbol{F}^{-c} \cdot \boldsymbol{n}_0 J dA_0 \tag{18}$$

The subscript $_0$ refers to the reference configuration.

Suppose that estimates are available of the positions $\boldsymbol{x}$ and the stresses. The estimates are marked by ' $\hat{}$ ' and the deviations of the estimates with respect to the actual situation by 'δ':

$$\boldsymbol{x} = \hat{\boldsymbol{x}} + \delta \boldsymbol{x} \qquad \boldsymbol{S} = \hat{\boldsymbol{S}} + \delta \boldsymbol{S} \qquad \boldsymbol{F} = \hat{\boldsymbol{F}} + \delta \boldsymbol{F} \tag{19}$$

With the use of:

$$\begin{aligned} &\hat{\boldsymbol{F}} = (\nabla_0 \hat{\boldsymbol{x}})^c \quad ; \ \det(\boldsymbol{F}) = \det(\hat{\boldsymbol{F}})(1 + \hat{\boldsymbol{F}}^{-1} : \delta \boldsymbol{F}) \\ &\delta \boldsymbol{F} = (\nabla_0 \delta \boldsymbol{x})^c \ ; \ \boldsymbol{F}^{-1} \approx (\boldsymbol{I} - \hat{\boldsymbol{F}}^{-1} \cdot \delta \boldsymbol{F}) \cdot \hat{\boldsymbol{F}}^{-1} \end{aligned} \tag{20}$$

and neglecting terms of order 2 and higher (18) transforms into:

$$\begin{aligned} &\int_{V_0} (\nabla_0 \boldsymbol{h})^c : (\hat{\boldsymbol{S}} \cdot \delta \boldsymbol{F}^c + \delta \boldsymbol{S} \cdot \hat{\boldsymbol{F}}^c) dV_0 = \\ &-\int_{A_0} \boldsymbol{h} \cdot \boldsymbol{\sigma}_{ext} \cdot \hat{\boldsymbol{F}}^{-c} \cdot \boldsymbol{n}_0 \hat{J} dA_0 - \int_{V_0} (\nabla_0 \boldsymbol{h})^c : (\hat{\boldsymbol{S}} \cdot \hat{\boldsymbol{F}}^c) dV_0 \end{aligned} \tag{21}$$

The right-hand-side of this equation represents the out-of-balance force, between the external forces and the internal forces, due to the deviations in the estimated positions $\hat{\boldsymbol{x}}$ and the estimated contractile element length $\hat{l}_c$.

As the stress $\boldsymbol{S}$ is the sum of the active and passive stress (see section 2) and the constitutive behaviour is known, the stress deviation $\delta \boldsymbol{S}$ can be rewritten as:

$$\begin{aligned} \delta \boldsymbol{S} &= \frac{\partial \boldsymbol{S}_p}{\partial \boldsymbol{E}} : \delta \boldsymbol{E} + \frac{\partial \boldsymbol{S}_a}{\partial l_s} \cdot \frac{\partial l_s}{\partial \boldsymbol{E}} : \delta \boldsymbol{E} + \frac{\partial \boldsymbol{S}_a}{\partial l_c} \delta l_c + \frac{\partial \boldsymbol{S}_a}{\partial t} \delta t \\ \delta \boldsymbol{E} &= \hat{\boldsymbol{F}}^c \cdot \delta \boldsymbol{F} \end{aligned} \tag{22}$$

3.2. Discretisation of the equations

As discretisation is extensively described by different authors (e.g. [13]) we will suffice in giving the results when using Galerkin's method.

Substituting (22) in (21) and applying discretisation results in:

$${}_1K_{ij}^{IJ} \delta x_j^J + {}_2K_{ij}^{IJ} \delta x_j^J + {}_3K_i^{IJ} (\delta l_c)^J + {}_4K_i^I (\delta t) = {}_1R_i^I + {}_2R_i^I \tag{23}$$

where:

$$ {}_1K_{ij}^{IJ} = \int_{V_0} \boxed{\hat{\boldsymbol{S}}_p + \hat{\boldsymbol{S}}_a} : \boldsymbol{b}^I \boldsymbol{e}_i \cdot \boldsymbol{b}^J \boldsymbol{e}_j dV_0 \tag{24} $$

$$ {}_2K_{ij}^{IJ} = \int_{V_0} \left(\hat{\boldsymbol{F}}^c \cdot \boldsymbol{e}_i \boldsymbol{b}^I\right) : \boxed{\frac{\partial \boldsymbol{S}_p}{\partial \boldsymbol{E}} + \left(\frac{\partial \boldsymbol{S}_a}{\partial l_s} \cdot \frac{\partial l_s}{\partial \boldsymbol{E}}\right)} : \left(\hat{\boldsymbol{F}}^c \cdot \boldsymbol{e}_j \boldsymbol{b}^J\right) dV_0 \tag{25} $$

$$ {}_3K_i^{IJ} = \int_{V_0} \frac{\partial \boldsymbol{S}_a}{\partial l_c} : \hat{\boldsymbol{F}}^c \cdot \boldsymbol{e}_i \boldsymbol{b}^I \psi^J dV_0 \tag{26} $$

$$ {}_4K_i^I = \int_{V_0} \frac{\partial \boldsymbol{S}_a}{\partial t} : \hat{\boldsymbol{F}}^c \cdot \boldsymbol{e}_i \boldsymbol{b}^I dV_0 \tag{27} $$

$$ {}_1R_i^I = \int_{A_0} \psi^I \boldsymbol{e}_i \cdot \boldsymbol{\sigma}_{ext} \cdot \hat{\boldsymbol{F}}^{-c} \cdot \boldsymbol{n}_0 \hat{J} dA_0 \tag{28} $$

$$ {}_2R_i^I = -\int_{V_0} \boxed{\hat{\boldsymbol{S}}_p + \hat{\boldsymbol{S}}_a} : \hat{\boldsymbol{F}}^c \cdot \boldsymbol{e}_i \boldsymbol{b}^I dV_0 \tag{29} $$

and $\psi^I(\xi)$ is the interpolation function of node I, x_i^I is the component of the position vector of node I in direction i, l_c^I the contractile element length at node I, $\boldsymbol{b}^I(\xi)$ the gradient of the interpolation function with respect to the reference configuration and $\boldsymbol{e}_i$ the unit vector in direction i.

3.3. Implementation in DIANA

The derived numerical formulation for muscle contraction is implemented in DIANA (version 5.1, development release). In essence the implementation means specifying the calculation of the stresses and stress derivatives in the 'boxed parts' of the equations (24) to (29).

The stress estimates $\hat{\boldsymbol{S}}_p$ and $\hat{\boldsymbol{S}}_a$ are calculated in the user subroutine `ELSGUS.F`. The passive stress $\hat{\boldsymbol{S}}_p$ is calculated using the strain estimate $\hat{\boldsymbol{E}}$ delivered by DIANA. The active stress $\hat{\boldsymbol{S}}_a$ depends on the sarcomere length l_s, time t and the contractile element length l_c (see equation (2) to (6)). The sarcomere length $l_s(t)$ is computed from the strain in the fiber direction. The time t is prescribed by defining a time dependent load table (see [10] vol.4). The length of the contractile element l_c is determined through numerical integration of equation (7), using an explicit Euler forward integration scheme:

$$ {}^0l_c(t) = l_c(t - \Delta t) + \Delta t \frac{dl_c}{dt}(t - \Delta t) \tag{30} $$

in the first iteration of a time-step. Every next iteration $n+1$ the estimate for $l_c(t)$ was improved using an implicit trapezium rule

$$ {}^{n+1}l_c(t) = l_c(t - \Delta t) + \frac{1}{2}\Delta t \left[v(t - \Delta t) + {}^n v(t)\right] \tag{31} $$

with

$$ {}^n v(t) = \frac{dl_c}{dt}(t, {}^n l_c(t), {}^n l_s(t)) \tag{32} $$

Equation (32) is computed from (7). The sarcomere length ${}^n l_s$ is computed from ${}^n l_s = l_{s,0}\sqrt{2\,({}^n \hat{E}_{11}) + 1}$. Each iteration the values of $l_c(t - \Delta t)$, ${}^n l_c$, $v(t - \Delta t)$ and ${}^n v(t)$ are stored on the FILOS-file. This time integration scheme was choosen, because it was easy to implement and appeared to be sufficiently accurate.

The tangential stiffness $\frac{\partial S_p}{\partial E} + \left(\frac{\partial S_a}{\partial l_s} \cdot \frac{\partial l_s}{\partial E}\right)$ is computed in the user subroutine `ELSEUS.F`. The contribution $\frac{\partial S_a}{\partial l_s} \cdot \frac{\partial l_s}{\partial E}$ can only be computed when $l_s(t)$, $l_c(t)$ and t are known. Again, l_s is computed from the strain in fiber direction. The time t is available and $l_c(t)$ is read from the FILOS-file where it was previously stored by the routine `ELSGUS.F`.

Part (27), which models the contribution of the deviation δt is neglected. The time steps are prescribed, so the error δt equals the time step Δt in the first iteration and is subsequently zero. In principle, this contribution could be taken into account through a force vector ${}_4K_i^I \delta t$ in the right-hand-side vector. As this is not possible using only the user subroutines `ELSGUS.F` and `ELSEUS.F` we decided to omit its contribution. Similar arguments hold for part (26), representing the contribution of the deviation δl_c. The consequence of these omissions is a slower convergence. Comparison with analytical solutions show no deviations.

4. Simulation of a papillary muscle experiment

Contractile properties of myocardial tissue can be investigated using papillary muscles in preload-afterload experiments [3, 5]. In these experiments the muscle is loaded with a certain preload, which causes the muscle to lengthen. Next, the muscle is stimulated, upon which it generates an active stress. When the stress exceeds a certain afterload the muscle shortens. When the active stress decays the muscle lengthens until the length equals the length in the preloaded condition. Subsequently the muscle relaxes at constant length.

The papillary muscle was modelled using one three-dimensional solid element with 8 nodes (element `HX24L` of DIANA [10]). The iteration scheme for the equilibrium iteration process was the regular Newton-Raphson method. A maximum of 20 iterations was allowed. The convergence criterium was set to `FORCE` and the relative out-of-balance force was set to 10^{-3}. The sarcomere reference length $l_{s,0}$ is $1.9\mu m$ [1]. We simulated an isometric, an isotonic, and a mixed isometric-isotonic contraction. Assuming homogeneity of the papillary muscle material properties, these experiments can be described by one nonlinear differential equation. The solution of this differential equation was used to check the DIANA results.

The isometric contraction corresponds to an afterload greater than the maximum stress generated by the muscle. Thus, the muscle length equals the preloaded length during the entire contraction. This is modelled by prescibing displacements at the ends of the muscle, so that sarcomere length increases from $1.9\mu m$ to $2.1\mu m$.

During the isotonic contraction the muscle shortens against a prescribed constant preload. The preload was chosen so that the muscle stretched from sarcomere length $1.9\mu m$ to $2.1\mu m$. The muscle was found to shorten by about 20%.

In the mixed isometric-isotonic contraction, the muscle contracts (1) isometri-

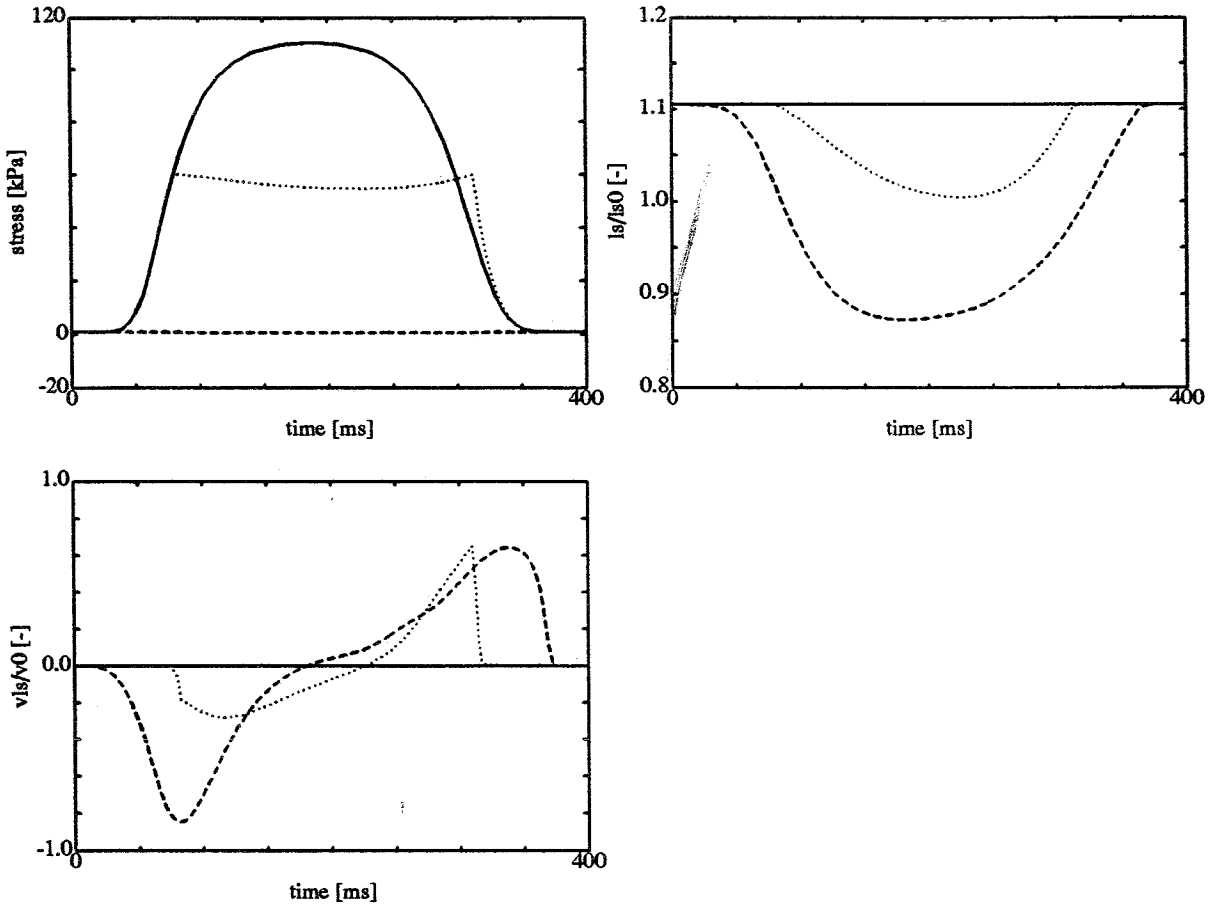

Fig. 2. Papillary muscle experiment: (a) Cauchy stress in the fiber direction v.s. time, (b) $l_s/l_{s,0}$ v.s. time, (c) v_{l_s}/v_0 v.s. time. (–) isometric contraction, (– –) isotonic contraction and (...) mixed isometric-isotonic contraction.

cally until the force equals a preset afterload. Next, the muscle contracts (2) isotonically against this constant afterload until the muscle relaxes and reaches its preload length. Subsequently the muscle relaxes isometrically (3). The isometric branch (1) was modelled by prescribing a force-time path which holds the muscle at constant length. This force-time path was determined from the isometric contraction. In the isotonic branch (2) the force was held constant and in the isotonic branch (3) another force-time path holds the muscle at constant length. The latter force-time path was prescribed according to the solution of the differential equation discussed above as it could not be determined from another simulation in DIANA due to the nonlinearities.

5. Discussion

With the formulation presented we are able to simulate myocardial muscle contraction. By integrating the contractile element length l_c and prescribing the time t it is not necessary to add degrees of freedom to the displacements. This gives two advantages: (1) the number of degrees of freedom is as little as possible and (2) the implementation can be held simple.

The implementation in finite element package DIANA could be accomplished in

the user subroutine **ELSGUS.F** and **ELSEUS.F**. As the contributions of the deviations δt and δl_c could not be taken in account in the user subroutines **ELSGUS.F** and **ELSEUS.F**, they were omitted. This may affect the rate of convergence, but does not affect the final solution.

As the simulations were performed using only one element and the deformation was homogeneous, the stability of the computation was always guaranteed. Stability of the computation has to be investigated in the case more elements are used and non-homogeneous deformation occurs. Possibly the contributions of δt via (27) and δl_c via (26) may not be neglected anymore.

6. Conclusions

We have implemented muscle contraction in the commercial finite element package DIANA, using only two user subroutines. Isometric contractions could be simulated very easily and the predicted stresses were accurate within 0.1 kPa or about 0.8%. The simulation of the isotonic contraction involved many iterations (> 10) for convergence, but again the predicted sarcomere lengths were accurate within $10^{-4}\mu m$ or 0.01%.

References

1. Arts, T., Veenstra, P.C., and Reneman, R.S. (1982). Epicardial deformation and left ventricular wall mechanics during ejection in the dog. *Am. J. Physiol.* 243:H379–H390.
2. Bovendeerd, P.H.M., Arts, T., Huyghe, J.M., van Campen, D.H., and Reneman, R.S. (1992). Dependence of local left ventricular wall mechanics on myocardial fiber orientation: a model study. *J. Biomech.* **25**, 1129–1140.
3. Brutsaert, D.L. and Sonnenblick, E.H. (1971) Nature of the force-velocity relation in heart muscle. *Cardiovascular Research*, supplement 1:18–33.
4. de Tombe, P.P. and ter Keurs, H.E.D.J. (1990). Force and velocity of sarcomere shortening in trabeculae from rat heart: effects of temperature. *Circ. Res.* 66:1239–1254.
5. Fung, Y.C. (1981). *Biomechanics: mechanical properties of living tissues*, chapter 9 and 10, pages 302–354. Springer-Verlag, New York.
6. Hill, A.V. (1938). The heat of shortening and the dynamic constants in muscle. *Proc. Roy. Soc. London* 126:136–165.
7. Nikolić, S., Yellin, E.L., Tamura, K., Vetter, H., Tamura, T., Meisner, J.S., and Frater, R.W.M. (1988). Passive properties of canine left ventricle: diastolic stiffness and restoring forces. *Circ. Res.* 62:1210–1222.
8. Snijders, J.M.A. (1994). *The triphasic mechanics of the intervertebral disc: a theoretical, numerical and experimental analysis.* PhD thesis, University of Limburg, Maastricht, The Netherlands.
9. ter Keurs, H.E.D.J., Rijnsburger, W.H., van Heuningen, R. and Nagelsmit, M.J. (1980). Tension development and sarcomere length in rat cardiac trabeculae: evidence of length-dependent activation. *Circ. Res.* 46:703–714.
10. TNO (1993). User's manual DIANA, vols 0, 1 and 4
11. van Heuningen, R., Rijnsburger, W.H., and ter Keurs, H.E.D.J. (1982). Sarcomere length control in striated muscle. *Am. J. Physiol.* 242:H411–H420.
12. Yin, F.C.P., Strumpf, R.K., Chew, P.H., and Zeger, S.L. (1987). Quantification of the mechanical properties of noncontracting canine myocardium under simultaneous biaxial loading. *J. Biomech.* 20:577–589.
13. Zienkiewics, O.C. and Morgan, K. (1983) *Finite Elements and Approximations.* John Wiley & Sons.